SPECTROSCOPY OF YTTRIUM SCANDATE DOPED WITH YTTERBIUM ION

O.K. Alimov, M.E. Doroshenko, E.A. Dobretsova, K.A. Pierpoint, S.Ya. Rusanov, V.V. Kashin, V.B. Tsvetkov

Prokhorov General Physics Institute of the Russian Academy of Sciences, Moscow 119991, Russia

Abstract

The spectral-kinetic properties of Yb^{3+} optical centers in $YScO_3$ crystal fiber were studied using selective laser spectroscopy. Various spectral characteristics of the Yb^{3+} optical centers were determined, including homogeneous and inhomogeneous broadening values, Stark level splitting, and the lifetime of Yb^{3+} ion optical centers. Three distinct types of Yb^{3+} optical centers were identified. The first optical center, with a lifetime of $\tau^{\mathbf{III}}_{\mathbf{77K}}$ = 4.05 ms, was formed due to the substitution of Y^{3+} for Yb^{3+} ions in the local site of C_{3i}. The other two Yb^{3+} optical centers, with lifetimes of $\tau^{\mathbf{I}}_{\mathbf{77K}}$ = 1.0 ms ($C^{\mathbf{II}}_2(Y^{3+})$ center) and $\tau^{\mathbf{II}}_{\mathbf{77K}}$ = 0.620 ms ($C^{\mathbf{II}}_2(Sc^{3+})$), respectively, were formed as a result of the substitution of Y^{3+} and Sc^{3+} for Yb^{3+} in the local site of C_2.

Key words: bixbyite, yttrium scandate, optical center, rare-earth ion, selective laser spectroscopy.

1. Introduction

Rare-earth doped sesquioxide materials have several advantageous properties, including high thermal conductivity [1–3], strong Stark-splitting [4–6], low phonon energies [7], as well as a wide transparency window ranging from 0.25 μm to 9.6 μm [8]. As a result, they are highly suitable for deployment in high-power solid-state lasers, particularly within the infrared wavelength range. Additionally, these materials can serve as alternatives to the widely used YAG crystals.

Yttrium oxide (Y_2O_3) and scandium oxide (Sc_2O_3) have been found to possess a cubic bixbyite-type structure [9,10]. These positions include the 8*b* site, which exhibits C_{3i} symmetry, and the 24*d* site, which has C_2 symmetry. Within the unit cell, there are three cations occupied the C_2 site, and one cation at the C_{3i} site. The overall crystal structure is formed by the arrangement two different 6-vertex polyhedra that share corners and edges. As a result, the crystal structure can be described as a chessboard packing arrangement, derived from the fluorite structural type.

Various rare-earth dopants in Y_2O_3 crystals have been studied, revealing that RE^{3+} ions can substitute of Y^{3+} in both the C_2 and C_{3i} structural sites [4,11–15]. Sc_2O_3 is an equally promising host material due to its high crystal field resulting from lattice distortions caused by the substitution of relatively small Sc^{3+} for large RE^{3+} ions [16–18].

Rare-earth sesquioxides have been found to exhibit different crystal structures [19–21], leading to variation in their laser properties depending on the specific rare-earth ion and host crystal structure. One of the $YScO_3$ phase modification, similar to Y_2O_3 and Sc_2O_3, possesses a bixbyite-type crystal structure [22]. In our works [10,23–25], $YScO_3$ (Y:Sc ratio is about 1:1) crystals were grown in the form of fibers using the laser-heated pedestal growth (LHPG) technique. This involved heating and melting the powder preform under CO_2 laser irradiation, followed by rapid cooling [26].

The luminescence and absorption spectra of bixbyite-like $YScO_3$ media doped with rare-earth ions include lines that are inhomogeneously broadened due to disorder in the crystal structure [27–30]. This characteristic makes these media highly promising for applications in ultrafast lasers and chirped pulse amplification. There are some publications on lasers based on single crystal and ceramic mixed sesquioxides doped by Nd^{3+} [31], Tm^{3+} [32–35], Ho^{3+} [36]. However, Yb^{3+}-doped materials can be an alternative to Nd^{3+}-doped active media for lasing in the range of 1 μm. Ytterbium-doped materials have a smaller quantum defect compared to neodymium materials, as well as a wider emission band [37–39]. Therefore, ytterbium-doped matrices are more suitable as active media in femtosecond lasers. Yb^{3+} ion with electronic configuration $^4f_{13}$ possesses one $^2F_{5/2}$ excited state with an energy range of 10200-11100 cm^{-1}, which is ideal for pumping with commercially available laser diodes emitting in the 915-980 nm range. This electronic level structure of Yb^{3+} excludes possible absorption from the $^2F_{5/2}$ excited state, as there are no higher energy levels available. Successful implementation of Yb lasers has been achieved in mixed sesquioxide ceramic hosts such as Yb^{3+}:$(Sc_xY_{1-x})_2O_3$ [40] and Yb^{3+}:$(Lu_xY_{1-x})_2O_3$ [41].

The investigation of RE^{3+}:$YScO_3$ mixed sesquioxide requires modern methods of selective laser spectroscopy. These methods enable the determination of quantitative features of optical centers and the identification of channels for both radiative and non-radiative energy [42]. Especially this applies to the transfer of excitation energy between the RE^{3+} optical centers, which are formed in the $YScO_3$ crystal fiber by substituting the positions of yttrium and scandium. The utilization of selective laser spectroscopy methods will allow for obtaining a complete characterization of the optical properties of RE^{3+} impurity center in $YScO_3$ crystal fiber and assessing the potential of this matrix as a laser-active medium.

Applying the laser-heated pedestal growth (LHPG) technique to obtain $YScO_3$ crystal fiber have been described in details earlier [10,24]. Features of the bixbyite-like crystal structure of $YScO_3$ have also been discussed in previous our research [10]. Additionally, the spectroscopic features of Nd^{3+} and Tm^{3+} dopants in $YScO_3$ crystal fibers have also been extensively investigated and published [10,23–25]. This current study aims to specifically focus on the spectral and kinetic properties of Yb^{3+}:$YScO_3$ crystal fibers using advanced selective laser spectroscopy methods.

2. Materials and Methods

Crystals of 0.1 at. % Yb^{3+}:$YScO_3$ were successfully grown using the laser-heated pedestal growth (LHPG) technique [10]. Commercial powders of Y_2O_3 and Sc_2O_3 of a purity of more than 99.999% (Sigma Aldrich, Burlington, MA, USA) were used as precursors, while Yb_2O_3 was used as activators. The crystals of Yb^{3+}:$YScO_3$ have been obtained in the form of a fiber with a diameter of 0.6 mm and a length of 50 mm. The crystal observed belongs to the bixbyite structural type and has a cubic structure with a space group of $Ia\overline{3}$.

The time-resolved luminescence excitation and luminescence spectra, as well as decay kinetics, were measured on the MDR-23 monochromator at temperatures of 77 K and 300 K. The FEU-83 и Hamamatsu R5108 photomultipliers were used as detectors. The Tektronix - TDS3052B broadband oscilloscope was used to record the time-resolved luminescence spectra and decay curve at the Solar LP-604 parametric generator excitation. The double spectral selection technique was used to record the decay curves accurately [42].

3. Results and Discussions

Figure 1 shows absorption spectra of $YScO_3$ crystal fiber doped with Yb^{3+} ions being measured at temperatures of 300 K and 77 K. The decrease in temperature from 300K to 77K results in narrowing of the absorption bands of Yb^{3+} ions, their structuring, and the emergence of new lines that were not visible at the higher temperature (300 K). Surprisingly, the number observed absorption lines (six ones) exceeds the expected number of three lines. This suggests the presence of additional Yb^{3+} optical centers within the crystal matrix, which contribute to the observed spectral overlap and the splitting and population of Stark components in the $^2F_{7/2}$ ground state. The existence of distinct optical centers of Yb^{3+} ions in other crystals like Y_2O_3 and Sc_2O_3 has been previously observed in [43].

The absorption spectrum of Yb^{3+}:$YScO_3$ crystal fiber was measured on the $^2F_{7/2} \rightarrow {}^2F_{5/2}$ transition of Yb^{3+} ion at a temperature of 77K. In Figure 1, curve 1 shows one narrow peak with a maximum at ν_{max} = 10246 cm^{-1}. Additionally, there are three broad bands with weakly resolved structure and maxima at 11111, 10753, and 10582 cm^{-1}. This spectrum is compared to the energy levels of Yb^{3+} ions with local symmetries of C_2 and C_{3i} in Y_2O_3 and Sc_2O_3 crystals as a reference [43]. The optical centers of Yb^{3+} ions in the Sc_2O_3 crystal exhibit the highest values of Stark splitting of the $^2F_{5/2}$ level being measured as ΔE = 856 cm^{-1} and ΔE = 1126 cm^{-1} for Yb^{3+} centers with local symmetries of C_2 (Figure 1*b*) and C_{3i} (Figure 1*d*), respectively. In Yb^{3+}:Y_2O_3, the Stark splitting values (ΔE) are equal to 726 $см^{-1}$ and 1062 $см^{-1}$ for Yb^{3+} optical centers with local symmetries of C_2

(Figure 1*a*) and C_{3i} (Figure 1*c*), respectively. Furthermore, in $YScO_3$ crystal fiber spectra, the Stark splitting of $^2F_{5/2}$ transition is determined to have a value of ΔE = 864 см$^{-1}$ (Figure 1, a curve 1).

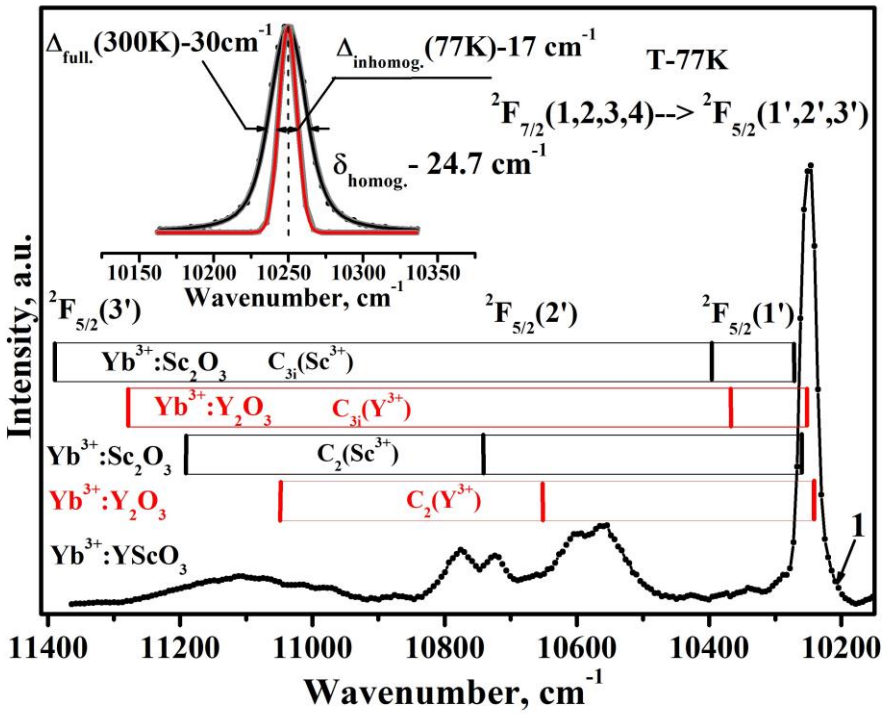

Figure 1. Absorption spectrum of Yb^{3+}-doped $YScO_3$ crystal fiber being measured at 77 K. Stark splitting of the $^2F_{5/2}$ transition of Yb^{3+} optical centers with a local symmetry of C_2 in Y_2O_3 (*a*) and Sc_2O_3 (*b*). Stark splitting of the $^2F_{5/2}$ transition of Yb^{3+} optical center with a local symmetry of C_{3i} in Y_2O_3 (*c*) and Sc_2O_3 (*d*) [43]. In the inset, absorption spectrum of the $^2F_{7/2}(1) \rightarrow {}^2F_{5/2}(1')$ resonance transition of Yb^{3+} ion in $YScO_3$ crystal fiber.

The analysis of the Stark splitting values for the $^2F_{5/2}(1', 2', 3')$ level in the sesquioxide materials reveals that the $YScO_3$ crystal fiber doped with Yb^{3+} ions exhibits splitting intermediate between the Yb^{3+}:Y_2O_3 and Yb^{3+}:Sc_2O_3 crystals. This observation is consistent with an intermediate lattice parameter value of the $YScO_3$ crystal fiber, as it is a solid solution. However, determining of the precise position of the Stark level components is complicated due to the presence of multiple types of Yb^{3+} optical centers in the $YScO_3$ crystal fiber, similar to those formed in Y_2O_3 and Sc_2O_3 crystals [43]. It is noteworthy that the absorption bands corresponding to the Stark components of the Yb^{3+} optical centers in $YScO_3$ exhibit broadening, which is presumably related to disorder in the crystal structure and the statistical distribution of Y^{3+} and Sc^{3+} ions in two structural positions, where they are partially substituted by Yb^{3+}. The spin-orbit interaction within the ^2F_J multiplet remains unchanged. In Figure 1, the Stark sublevels associated with the $^2F_{5/2}$ excited state denoted by bars,

and the sublevels of the $^2F_{7/2}$ ground state are represented by unbarred numbers. The numbering of levels within the multiplet follows a bottom-to-top sequence.

To analyze the shape of the absorption band of the $^2F_{7/2}(1) \rightarrow {}^2F_{5/2}(1')$ transition and evaluate the value of homogeneous and inhomogeneous broadening in the Yb^{3+}:$YScO_3$ crystal, the $^2F_{7/2}(1) \rightarrow {}^2F_{5/2}(1')$ transition was singled out from the overall spectrum taken at 77 K and 300K. Figure 1 shows the optical absorption spectrum (curve 1) of the Yb^{3+}:$YScO_3$ crystal fiber being measured at 77K. The absorption line according to the $^2F_{7/2}(1) \rightarrow {}^2F_{5/2}(1')$ transition of Yb^{3+} ions in the crystal fiber is shown in the inset of Figure 1 where the half-width of the transition line is indicated by horizontal arrows. The absorption line of the $^2F_{7/2}(1) \rightarrow {}^2F_{5/2}(1')$ transition being measured at 300K appears symmetrical and exhibits a peak at a frequency of ν_{max} = 10246 cm^{-1}. The full width of the transition at half height, Δ_{full} (300 K), was determined to be 30 cm^{-1} by approximating the line with a Voigt distribution function [44]. Lowering the temperature to 77 K causes the absorption line to narrow to a value of Δ'(77K) = 17 cm^{-1} at the instrumental function of R_A = 2 cm^{-1}. The absorption lines of the $^4F(1) \rightarrow {}^4F_{5/2}(1')$ transition were fitted using a Gaussian distribution function. Using the equation derived in in the work [44], the value of the homogeneous broadening of the $^4F_{7/2}(1) \rightarrow {}^4F_{5/2}(1')$ transition was calculated to be $\delta(300K) = [\Delta^2_{full}(300K) - (\Delta')^2_{inhomog}(77K)]^{1/2}$ = 24.7 cm^{-1}.

To gain a more comprehensive understanding of the mechanism behind the formation of Yb3+ optical centers in $YScO_3$, we measured luminescence decay kinetics at a temperature of 77K (Figure 2). The excitation of ytterbium ions was performed specifically on the $^2F_{7/2}(1) \rightarrow {}^2F_{5/2}(1')$ resonance transition. Subsequently, the resulting fluorescence signals were analyzed by determining the fluorescence lines with peak values at νdet. = 9737, 9634, 9320, and 8985 cm^{-1}.

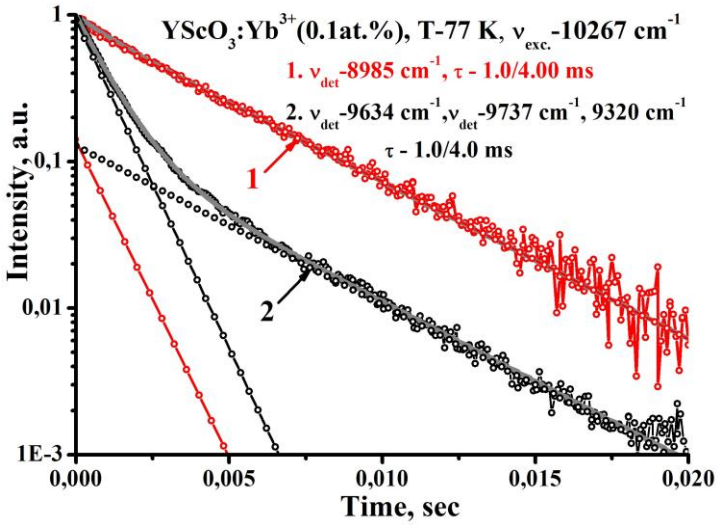

Figure 2. Luminescence decay kinetics of Yb^{3+} ions in $YScO_3$. Excitation of Yb^{3+} ions was carried out on the $^2F_{7/2}(1) \rightarrow {}^2F_{5/2}(1')$ transition at $\nu_{exc.}$ = 10267 cm^{-1}. The detection was then performed at frequencies of $\nu_{det.}$ = 8985 cm^{-1} (curve 1) and $\nu_{det.}$ = 9737, 9634, 9320 cm^{-1} (curve 2).

The decay luminescence curves (Fig. 2, curves 1, 2) can be better characterized by considering them as a sum of two exponentials with lifetimes of 1.0 and 4.0 ms. The relative contribution of the long-lived or short-lived components in the total intensity of Yb^{3+} luminescence varies depending on the detection frequency. In the $YScO_3$ crystal structure, Yb^{3+} optical centers with a lifetime of τ = 1.0 ms are formed when Yb^{3+} substitutes of Y^{3+} in the C_2 site. The intensity of the short-lived component increases when registering the decay kinetics of Yb^{3+} luminescence on the line belonging to the long-lived center ($\nu_{det.}$ = 9737 cm^{-1}). This increase is caused by the overlap of the luminescence bands with peaks of $\nu_{max.}$ = 9737 cm^{-1} and 9625 cm^{-1}. This overlapping leads to a combined effect on the luminescence intensity, resulting in a change in the relative contribution of the short-lived component. On the other hand, when the detection frequency is ν_{det} = 8985 cm^{-1}, the decay kinetics of Yb^{3+} luminescence can be accurately described by a single exponential decay law (Fig. 2, curve 1). This detection band corresponds to a long-lived optical center with a lifetime of τ = 4.0 ms. This long-lived center is formed when Yb^{3+} substitutes with Y^{3+} in the C_{3i} site.

Figure 3 shows luminescence decay kinetics being measured on the $^2F_{7/2}(1) \rightarrow {}^2F_{5/2}(1')$ transition in Yb^{3+}:$YScO_3$ at excitation of $\nu_{exc.}$= 10235 $см^{-1}$ and a temperature of 77 K. The luminescence of the Yb^{3+} ion in $YScO_3$ was recorded on the $^2F_{5/2}(1') \rightarrow {}^2F_{5/2}(2, 3, 4)$ transition at frequencies of 9891, 9775, and 9653 cm^{-1}. The luminescence decay curve being measured at 77K was described by a single exponential decay law with a lifetime of τ = 0.620 ms, indicating the presence of a second short-lived optical center with a local symmetry of C_2 in the crystal fiber. This center is formed in the matrix through the substitution of scandium ions with ytterbium ions.

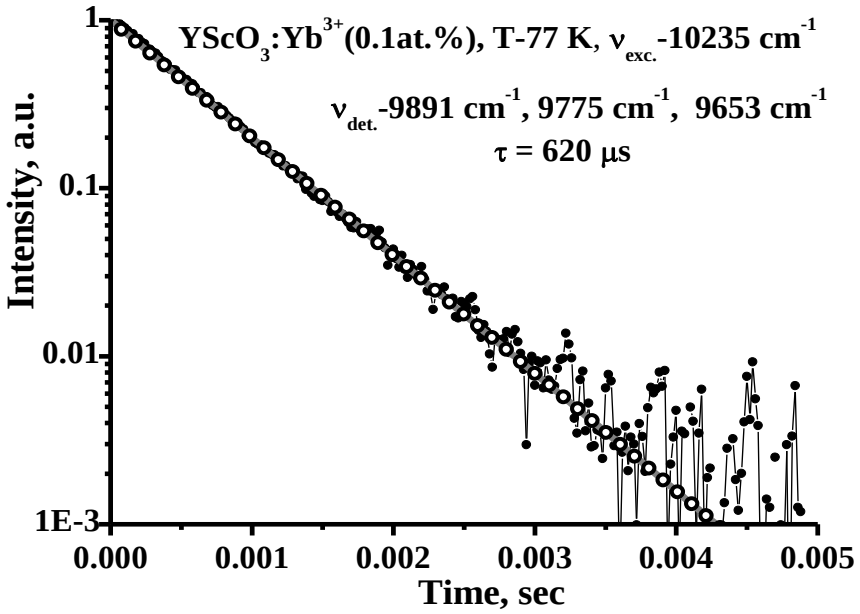

Figure 3. Luminescence decay kinetics being measured on the $^2F_{7/2}(1) \rightarrow {}^2F_{5/2}(1')$ transition of Yb^{3+} ions in $YScO_3$ at an excitation of 10235 cm^{-1}. The luminescence decay curve was registered at frequencies of $\nu_{det.}$ = 9891, 9775, and 9653 cm^{-1}.

The difference in lifetimes of the two short-lived centers is due to the difference in ionic radii of Y^{3+} (0.87 Å) and Sc^{3+} (0.75 Å), which are replaced by Yb^{3+} (1.01 Å) in the C_2 site. The substitution of yttrium or scandium ions in the lattice with ytterbium ion leads to a change in the distance between the cation and its oxygen environment in the distorted octahedron [45–47]. Decreasing the distance between the impurity center and its oxygen environment lead to changes in the crystal field parameters that are responsible for the probabilities of radiative transitions[42]. Therefore, the optical center with a lifetime of 0.620 ms is attributed to the substitution of Sc^{3+} with C_2 site symmetry in the $YScO_3$ crystal lattice for Yb^{3+}, and the optical center being formed due to the substitution of Y^{3+} with C_2 site symmetry in the $YScO_3$ crystal lattice for Yb^{3+} has a longer lifetime (1.0 ms).

To confirm the existence of at least two types of Yb^{3+} optical centers in $YScO_3$, the time-resolved luminescence spectra were measured (Figure 3). By increasing the time delay (t_{del}) from 40 μs to 1.58 ms, the intensities of the Yb^{3+} ion fluorescence lines with maxima at $\nu_{max.}$ = 9775, 9632, 9320 cm^{-1} were redistributed. Specifically, an increase in intensity was observed for the luminescence line with maxima at $\nu_{max.}$ = 9737 and 9320 cm^{-1}, while a decrease in intensity was observed for the line with maxima at $\nu_{max.}$ = 9625 cm^{-1}.

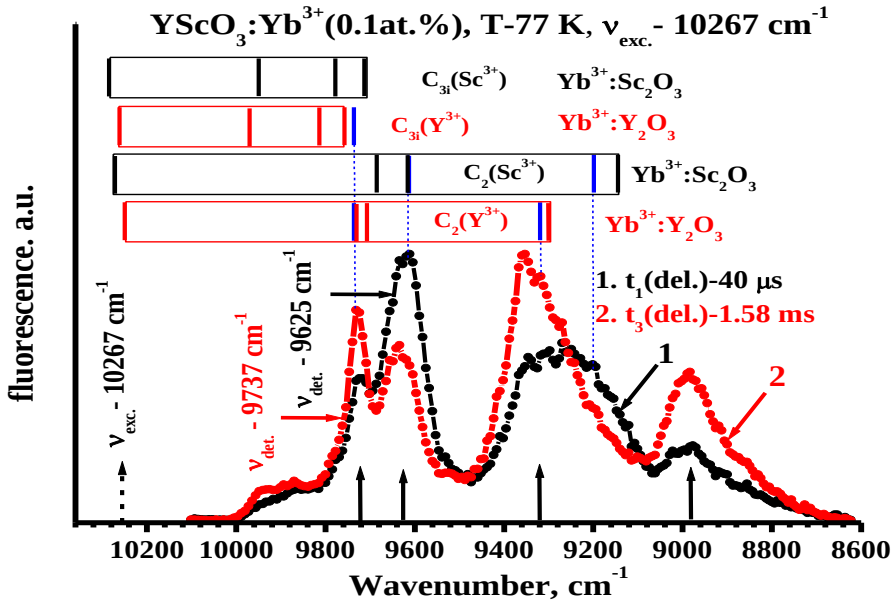

Figure 4. Time-resolved luminescence spectra of ytterbium ions in $YScO_3$ being measured at time delays of $t_{1(del.)}$ = 40 μs (curve 1) and $t_{3(del.)}$ = 1.58 ms (curve 2). The observed luminescence decay kinetics were recorded at specific frequencies, as indicated by the arrows. Stark splitting of the $^2F_{7/2}$ level of Yb^{3+} optical centers with local symmetry of C_2 and C_{3i} in Y_2O_3 (red one) and Sc_2O_3 (black one) crystals [43].

The number of luminescence lines being obtained on the $^2F_{5/2} \rightarrow {}^2F_{7/2}$ transition of Yb^{3+} is five, that exceeds the calculated value (four), therefore, there are at least two types of optical centers of the ytterbium ion in the $YScO_3$ crystal fiber. As shown in the works [43], two types of optical centers exist in both Y_2O_3 and Sc_2O_3 crystals doped with Yb^{3+} ions: a) low-symmetric in the C_2 site, and b) high-symmetric one in the C_{3i} site. The Stark component energies for these two types of Yb^{3+} optical centers in both Y_2O_3 and Sc_2O_3 crystals are obtained at T=10K in [40] and shown in Figure 4. The largest splitting of the $^2F_{7/2}$ level is observed for the center with C_2 local symmetry in the Sc_2O_3 crystal. Calculations on crystal field theory have been performed in [41] to determine the Stark component energies and the the $^2F_{7/2}$ and $^2F_{5/2}$ for Yb3+ ions in the Y_2O_3, yielding results that are in good agreement with previous studies [40].

Figure 5 shows the luminescence spectra being measured on the $^2F_{7/2}(1) \rightarrow {}^2F_{5/2}(1')$ transition of Yb^{3+} ion at an excitation of $\nu_{exc.}$ = 10235 cm^{-1} and a temperature of T = 77 K. When the time delay is changed from $t_{1(del)}$ = 40 μs to $t_{3(del)}$ = 1.6 ms, there is no significant change observed in the luminescence spectra, particularly in the spectral line with a maximum at ν_{max} = 9653 cm^{-1}. Weak lines with maxima at ν_{max} = 9891, 9775, and 9653 cm^{-1} are observed on the short-wavelength side of the luminescence spectrum. Increasing the time delay up to t_{del} = 1.6 ms results in a slight shift of the luminescence line with a maximum at λ_{max} = 1036 nm, a decrease in the intensity of the band with a

maximum at v_{max} = 9225 cm^{-1}, and appearance of a weak luminescence line with a maximum at v_{max} = 8834 cm^{-1}.

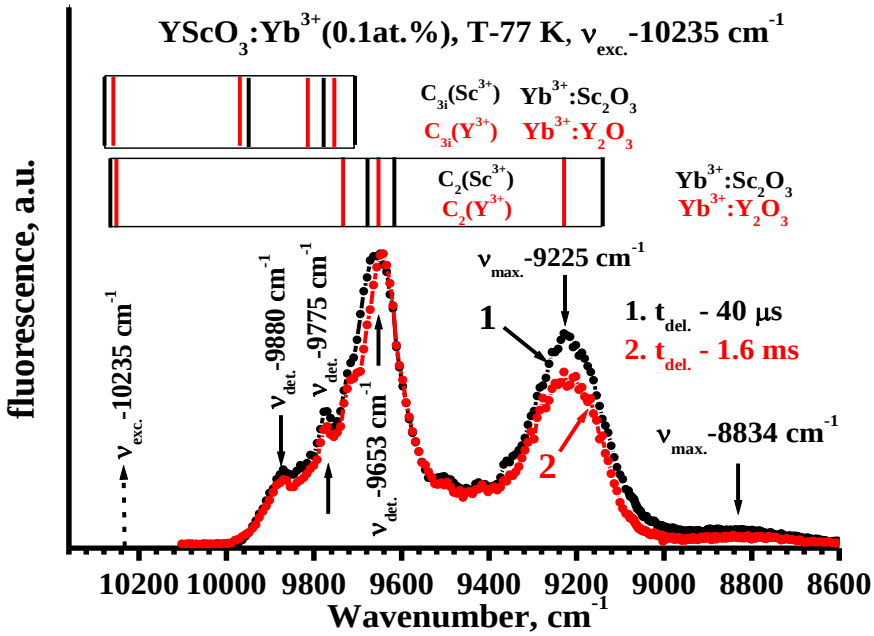

Figure 5. Time-resolved luminescence spectra of Yb^{3+} ions in $YScO_3$ being measured at temperature of T = 77 K and time delays of t_1 = 40 μs (curve 1) and t_3 = 1.6 ms (curves 2). Stark component energies of the $^2F_{7/2}$ level for Yb^{3+} optical centers with local symmetries of C_2 and C_{3i} in both Y_2O_3 (red one) and Sc_2O_3 (black one) crystals [43].

These factors suggest the presence of a dominant short-lived Yb^{3+} optical center in $YScO_3$. This is confirmed by the kinetic studies shown in Figure 3. The energies of Stark components of Yb^{3+} ion in both Y_2O_3 and Sc_2O_3 crystals, corresponding to two types of optical centers with a local symmetry of C_2 and C_{3i}, were determined in previous work [43] at a temperature of T = 10 K are shown in Figure 5. Here, the red lines indicate the positions of Yb^{3+} ion Stark components in Y_2O_3, while the black lines represent positions of Yb^{3+} in Sc_2O_3. Based on the kinetic and spectral measurements carried out for Yb^{3+}:$YScO_3$ it has been determined that there are three types of Yb^{3+} optical centers in the $YScO_3$ crystal fiber. Two of them with a local symmetry of C_2 labeled as C_2^{II} (Y^{3+}) and C_2^{II}(Sc^{3+}) correspond to substitution of Y^{3+} and Sc^{3+} cations with Yb^{3+}, respectively. The third one with a high symmetry of C_{3i} labeled as C_{3i}(Y^{3+}) corresponds to substitution of Y^{3+} with Yb^{3+}. The position of the Stark components of the Yb^{3+} optical centers in $YScO_3$ crystal have been determined based on the obtained results.

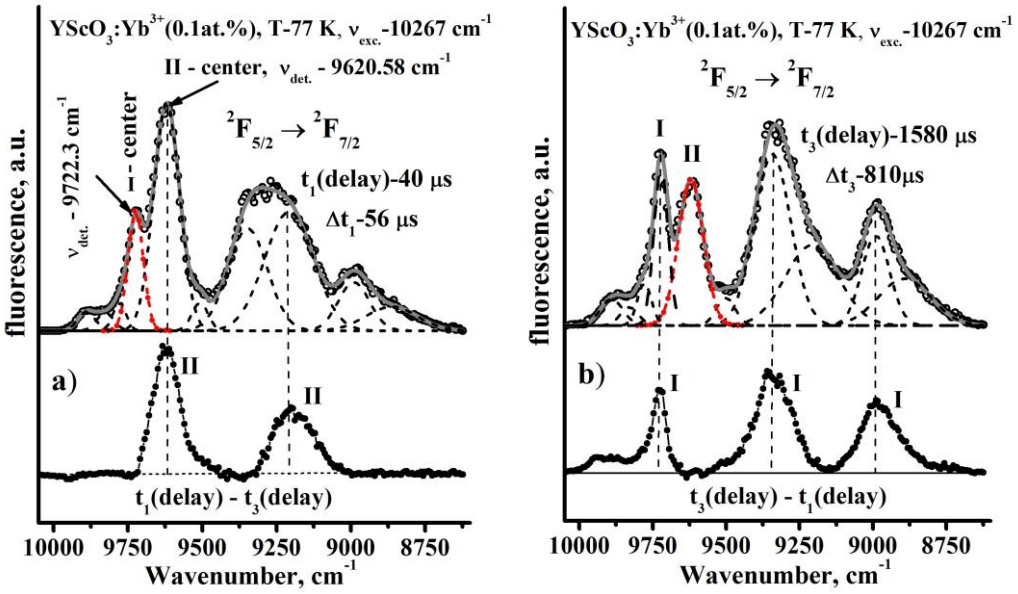

Figure 6. Low-temperature (77 K) time-resolved luminescence spectra being measured on the $^2F_{5/2} \rightarrow {}^2F_{7/2}$ transition of Yb^{3+} ions in the $YScO_3$ crystal fiber at two different time delays of: (*a*) $t_{1(del.)}$ = 40 μs (*a*) and $t_{3(del.)}$ = 1.58 ms (*b*). The luminescence spectra of Yb^{3+} ions were normalized to the lines with maxima at 9737 and 9625 cm^{-1} being obtained at the time delays of $t_{1(del.)}$ = 40 μs and (*b*) $t_{3(del.)}$ = 1.58 ms, respectively. The difference spectra of luminescence [t1(del.) - t3(del.)] and [t3(del.) - t1(del.)] are shown at the bottom of (*a*) and (*b*), respectively.

The luminescence spectra (Figure 4, curves 1 and 2) have been normalized based on the spectral lines at frequencies oof ν_{max} = 9737 cm^{-1} and ν_{max} = 9625 cm^{-1} (Figure 6*a* and *b*, highlighted in red on the spectra). Time delays of $t_{1(del.)}$ = 40 μs and $t_{3(del.)}$ = 1.58 ms were used to measure the luminescence spectra. To analyze the spectra, a Gaussian distribution function was employed to separate the spectral components. Surprisingly, six spectral lines were observed instead of the expected three (excluding the main inter-Stark $^2F_{5/2}(1) \rightarrow {}^2F_{7/2}(1')$ transition).

The luminescence spectrum obtained at a short time delay ($t_{1(del.)}$ = 40 μs) was subtracted from the spectrum taken with a long-time delay ($t_{3(del.)}$ = 1.58 ms). So, the positions of two lines associated with the short-lived ytterbium center can be identified (Figure 6a, bottom). Similarly, the spectrum obtained at a long time delay was subtracted from the spectrum taken with a short time delay, that reveals the positions of the spectral lines corresponding to the long-lived center (Figure 6a, bottom). The number of luminescence lines corresponds to the calculated number of the Stark components of the $^2F_{7/2}(1, 2, 3, 4)$ level of the long-lived center. The position of the Stark components of Yb^{3+} ions in the $YScO_3$ crystal is shown in Figure 4 and 5 (blue line), serving as a basis for assigning the luminescence lines to optical centers with local symmetries of C_2 and C_{3i}. According to Figure 4, the luminescence spectral lines of Yb^{3+} ions belong to optical centers with local

symmetries of C_2 (Y^{3+}), C_{3i} (Y^{3+}), and C_2 (Sc^{3+}). In the case of a single low-symmetry center II (Yb^{3+}), the luminescence spectra of the ytterbium ion can be attributed to optical centers with local symmetries of C_2 (Sc^{3+}) and C_2 (Y^{3+}), which lines are overlapped (see Figure 5).

Figure 7 shows the impact of excitation frequency (curves 1, 2, 3) on the time-resolved luminescence spectra being measured on the $^2F_{5/2}(1) \rightarrow {}^2F_{7/2}(1', 2', 3')$ transition of Yb^{3+} short-lived optical centers (II(Y^{3+}) and II(Sc^{3+})). Analysis reveals that the luminescence spectra exhibit distinctive shift at various excitation frequencies. Notably, the maximum observed shift, denoted as $\Delta E \sim 30$ cm^{-1}, can be observed.

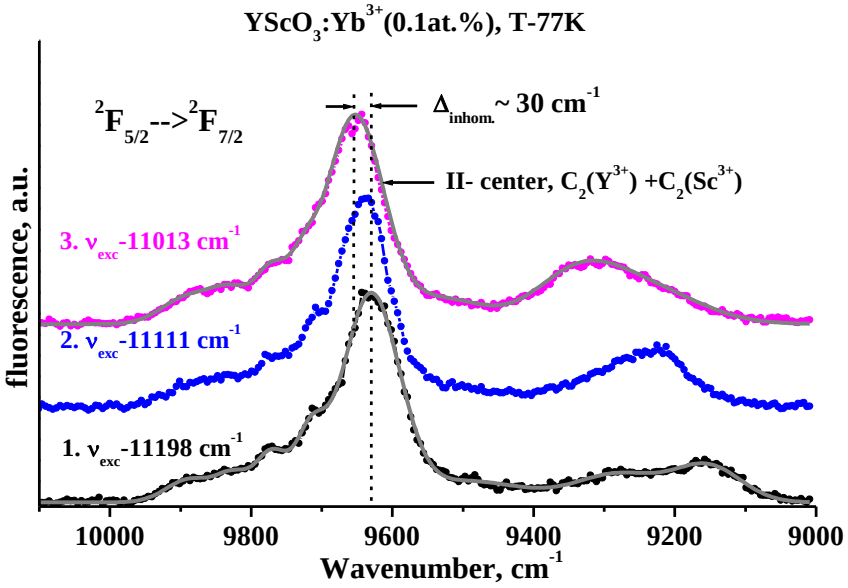

Figure 7. Time-resolved luminescence spectra being measured on the $^2F_{7/2} \rightarrow {}^2F_{5/2}$ transition of ytterbium ions in the $YScO_3$ crystal fiber (curves 1, 2, 3). These spectra were observed at a time delay of $t_{1(del.)} = 40$ μs and a temperature of 77 K. The luminescence measurements were performed using excitation frequencies of 11198 cm^{-1}, 11111 cm^{-1}, and 11013 cm^{-1}, corresponding to curves 1, 2, and 3, respectively.

The observed shift in the maxima of the short-lived center and the dependence of the luminescence spectra on excitation suggest the presence of disorder in the $YScO_3$ crystal fiber matrix of the crystal fiber. The degree of disorder in the optical center II of Yb3+ ions is influenced by the inhomogeneous broadening of the luminescence and absorption lines. In the long-wavelength wing of the Yb^{3+} ion luminescence spectrum (Figure 7), the bands associated with C^{II}_2 (Y^{3+}, Sc^{3+}) symmetrical centers (Fig. 3a, b) exhibit varying intensity and spectral position on the $^2F_{5/2}(1', 2') \rightarrow {}^2F_{7/2}(2, 3, 4)$ inter-Stark transitions, depending on the excitation wavelength. The spectral shift and intensity change of these Yb^{3+} bands are determined by the efficient excitation of the C^{II}_2 (Y^{3+}) and C^{II}_2 (Sc^{3+}) centers. It is worth noting that simultaneous excitation of Yb^{3+} optical centers (C^{II}_2 (Y^{3+})

and C^{II}_2 (Sc^{3+})), which have a heterogeneous distribution within a single optical center, can also occur (Figure 7, curve 3). This observation can be attributed to the close proximity and spectral overlap of the Stark energy levels associated with the 2F7/2 → 2F5/2 absorption transition of two distinct optical centers, II(Y3+) and II(Sc3+), with the C_2 local symmetry.

4. Conclusions

The spectral-kinetic properties of Yb^{3+} optical centers in $YScO_3$ crystal fiber were investigated using selective laser spectroscopy methods. The quantitative spectral characteristics of Yb^{3+} optical centers were determined: homogeneous broadening (δ(300K) = 24.7 cm^{-1}), inhomogeneous broadening ($\Delta'_{inhom.}$(77K) = 17 cm^{-1}), Stark splitting, and lifetimes of Yb^{3+} optical centers.

Three types of Yb^{3+} optical centers of ions have been found in $YScO_3$. The first one is a highly symmetric optical center with a local symmetry C_{3i}(Y^{3+}) and a lifetime of τ^{I}_{77K} = 4.0 ms, which is formed as a result of substitution of Y^{3+} ions for ytterbium ions in the crystal lattice. The second center has local symmetry C_2^{II} (Y^{3+}) and a lifetime of τ_{77K}^{II} = 1.0 ms. The third one is a low-symmetry C_2^{II} (Sc^{3+}) center with lifetimes of τ_{77K}^{II} = 0.620 ms.

It has been shown that the broadening of the absorption and luminescence spectra of the Yb^{3+} optical centers with local symmetry C_2^{II} (Y^{3+}) and C_2^{II} (Sc^{3+}) in $YScO_3$ is due to the disorder in the $YScO_3$ crystal structure.

Funding: This research was funded by the Russian Science Foundation, grant number 22-22-00968.

Conflicts of Interest: The authors declare no conflict of interest.

1. Alombert-Goget, G.; Guyot, Y.; Guzik, M.; Boulon, G.; Ito, A.; Goto, T.; Yoshikawa, A.; Kikuchi, M. Nd3+-Doped Lu2O3 Transparent Sesquioxide Ceramics Elaborated by the Spark Plasma Sintering (SPS) Method. Part 1: Structural, Thermal Conductivity and Spectroscopic Characterization. In Proceedings of the Optical Materials; 2015; Vol. 41.
2. Petermann, K. Oxide Laser Crystals Doped with Rare Earth and Transition Metal Ions. In *Handbook of Solid-State Lasers: Materials, Systems and Applications*; 2013; pp. 3–27.
3. Klein, P.H.; Croft, W.J. Thermal Conductivity, Diffusivity, and Expansion of Y2O 3, Y3 Al5O12, and LaF3 in the Range 77°-300°K. *J Appl Phys* **1967**, *38*, 1603, doi:10.1063/1.1709730.
4. Gruber, J.B.; Nash, K.L.; Sardar, D.K.; Valiev, U. V.; Ter-Gabrielyan, N.; Merkle, L.D. Modeling Optical Transitions of Er3+ (4f11) in C 2 and C3i Sites in Polycrystalline Y2O 3. *J Appl Phys* **2008**, *104*, doi:10.1063/1.2955445.
5. Jayswal, S.; Ningthoujam, R.S.; Moirangthem, R.S. Observation of Stark Splitting in Micro Upconversion Photoluminescence Spectra of Polycrystalline Ln3+ Doped Y2O3microspheres. *Nanotechnology* **2022**, *33*, doi:10.1088/1361-6528/ac6cf7.

6. Simura, R.; Jouini, A.; Mun, J.H.; Brenier, A.; Yoshikawa, A.; Boulon, G.; Fukuda, T. Growth and Spectroscopic Properties of Yb3+-Doped Sc2O3 Crystals Grown by the Micro-Pulling-down Method. *Opt Mater (Amst)* **2007**, *30*, doi:10.1016/j.optmat.2006.11.047.
7. Dilawar, N.; Mehrotra, S.; Varandani, D.; Kumaraswamy, B. V.; Haldar, S.K.; Bandyopadhyay, A.K. A Raman Spectroscopic Study of C-Type Rare Earth Sesquioxides. *Mater Charact* **2008**, *59*, doi:10.1016/j.matchar.2007.04.008.
8. Harris, D.C.; Cambrea, L.R.; Johnson, L.F.; Seaver, R.T.; Baronowski, M.; Gentilman, R.; Scott Nordahl, C.; Gattuso, T.; Silberstein, S.; Rogan, P.; et al. Properties of an Infrared-Transparent MgO: Y2O3 Nanocomposite. *Journal of the American Ceramic Society* **2013**, *96*, doi:10.1111/jace.12589.
9. Moore, P.B.; Araki, T. Braunite: Its Structure and Relationship Insights on the Genealogy of to Bixbyite , and Some Fluorite Derivative Structures. *American Mineralogist* **1976**, *61*, 1226–1240.
10. Alimov, O.; Dobretsova, E.; Guryev, D.; Kashin, V.; Kiriukhina, G.; Kutovoi, S.; Rusanov, S.; Simonov, S.; Tsvetkov, V.; Vlasov, V.; et al. Growth and Characterization of Neodymium-Doped Yttrium Scandate Crystal Fiber with a Bixbyite-Type Crystal Structure. *Cryst Growth Des* **2020**, *20*, 4593–4599, doi:10.1021/acs.cgd.0c00389.
11. Gruber, J.B.; Krupke, W.F.; Poindexter, J.M. Crystal-Field Splitting of Trivalent Thulium and Erbium J Levels in Yttrium Oxide. *J Chem Phys* **1964**, *41*, 3363, doi:10.1063/1.1725734.
12. Morrison, C.A.; Leavitt, R.P.; Gruber, J.B.; Chang, N.C. Optical Spectra, Energy Levels, and Crystal-Field Analysis of Tripositive Rare-Earth Ions in Y2O3. III. Intensities and g Values for C2 Sites. *J Chem Phys* **1983**, *79*, 4758, doi:10.1063/1.445619.
13. Gruber, J.B.; Leavitt, R.P.; Morrison, C.A.; Chang, N.C. Optical Spectra, Energy Levels, and Crystal-Field Analysis of Tripositive Rare-Earth Ions in Y2O3. IV. C3i Sites. *J Chem Phys* **1984**, *82*, 5373, doi:10.1063/1.448621.
14. Leavitt, R.P.; Gruber, J.B.; Chang, N.C.; Morrison, C.A. Optical Spectra, Energy Levels, and Crystal-Field Analysis of Tripositive Rare-Earth Ions in Y2O3. II. Non-Kramers Ions in C 2 Sites. *J Chem Phys* **1981**, *76*, 4775, doi:10.1063/1.442796.
15. Chang, N.C.; Gruber, J.B.; Leavitt, R.P.; Morrison, C.A. Optical Spectra, Energy Levels, and Crystal-Field Analysis of Tripositive Rare Earth Ions in Y2O3. I. Kramers Ions in C2 Sites. *J Chem Phys* **1982**, *76*, 4775, doi:10.1063/1.443530.
16. Merkle, L.D. Rare-Earth-Doped Laser Materials: Spectroscopy and Laser Properties. In Proceedings of the Materials Research Society Symposium Proceedings; 2012; Vol. 1471.
17. Moncorgé, R.; Guyot, Y.; Kränkel, C.; Lebbou, K.; Yoshikawa, A. Mid-Infrared Emission Properties of the Tm3+-Doped Sesquioxide Crystals Y2O3, Lu2O3, Sc2O3 and Mixed Compounds (Y,Lu,Sc)2O3 around 1.5-, 2- and 2.3-Mm. *J Lumin* **2022**, *241*, 118537, doi:10.1016/j.jlumin.2021.118537.
18. Fornasiero, L.; Mix, E.; Peters, V.; Heumann, E.; Petermann, K.; Huber, G. Efficient Laser Operation of Nd:Sc2O3 at 966 Nm, 1082nm and 1486nm.; 2014.
19. Zinkevich, M. Thermodynamics of Rare Earth Sesquioxides. *Prog Mater Sci* 2007, *52*.
20. Rahm, M.; Skorodumova, N. V. Phase Stability of the Rare-Earth Sesquioxides under Pressure. *Phys Rev B Condens Matter Mater Phys* **2009**, *80*, doi:10.1103/PhysRevB.80.104105.
21. Irshad, K.A.; Srihari, V.; Kalavathi, S.; Shekar, N.V.C. Structural Phase Transition, Equation of State and Phase Diagram of Functional Rare Earth Sesquioxide Ceramics (Eu1−xLax)2O3. *Sci Rep* **2020**, *10*, doi:10.1038/s41598-020-68400-9.
22. Giaquinta, D.M.; Loye, H.C. zur Structural Predictions in the ABO3 Phase Diagram. *Chemistry of Materials* 1994, *6*.
23. Dobretsova, E.; Alimov, O.; Guryev, D.; Voronov, V.; Rusanov, S.; Kashin, V.; Kutovoy, S.; Vlasov, V.; Badyanova, L.; Novikov, I.; et al. Structural and Spectroscopic Features of the Bixbyite-Type Yttrium Scandate Doped by Rare-Earth Ions. *Crystals (Basel)* **2022**, *12*, 1745, doi:10.3390/cryst12121745.
24. Dobretsova E. A.; Alimov O. K.; Rusanov S. Ya.; Kashin V. V.; Voronov V. V.; Guryev D. A.; Kutovoi S. A.; Vlasov V. I.; Tsvetkov V. B. Spectroscopy of the Yttrium Scandate Doped by Thulium Ions. *Physics of the Solid State* **2022**, *64*, 2238, doi:10.21883/pss.2022.14.54426.22s.
25. Dobretsova, E.; Alimov, O.; Rusanov, S.; Kashin, V.; Tsvetkov, V. Selective Laser Spectroscopy of the Bixbyite-Type Yttrium Scandate Doped by Rare-Earth Ions. *Materials* **2023**, *16*, doi:10.3390/ma16216829.

26. Bufetova, G.A.; Kashin, V. V; Nikolaev, D.A.; Rusanov, S.Y.; Seregin, V.F.; Tsvetkov, V.B.; Shcherbakov, I.A.; Yakovlev, A.A. Neodymium-Doped Graded-Index Single-Crystal Fibre Lasers. *Quantum Elec (Woodbury)* **2006**, *36*, 616, doi:10.1070/qe2006v036n07abeh013176.
27. Guo, R.; Huang, D.; Lu, D.; Liang, F.; Zhang, Q.; Yu, H.; Zhang, H. Spectral Broadening Mechanism of Yb 3+ -Doped Cubic Lu x Sc 2-x O 3 Sesquioxide Crystals for Ultrafast Lasers . *Opt Mater Express* **2022**, *12*, doi:10.1364/ome.451476.
28. Kränkel, C.; Uvarova, A.; Guguschev, C.; Kalusniak, S.; Hülshoff, L.; Tanaka, H.; Klimm, D. Rare-Earth Doped Mixed Sesquioxides for Ultrafast Lasers [Invited]. *Opt Mater Express* **2022**, *12*, 1074–1091, doi:10.1364/ome.450203.
29. Liu, W.; Lu, D.; Pan, S.; Xu, M.; Hang, Y.; Yu, H.; Zhang, H.; Wang, J. Ligand Engineering for Broadening Infrared Luminescence of Kramers Ytterbium Ions in Disordered Sesquioxides. *Cryst Growth Des* **2019**, *19*, 3704–3713, doi:10.1021/acs.cgd.9b00034.
30. Liu, W.; Lu, D.; Guo, R.; Wu, K.; Pan, S.; Hang, Y.; Sun, D.; Yu, H.; Zhang, H.; Wang, J. Broadening of the Fluorescence Spectra of Sesquioxide Crystals for Ultrafast Lasers. *Cryst Growth Des* **2020**, *20*, 4678–4685, doi:10.1021/acs.cgd.0c00473.
31. Li, D.; Liu, J.; Xu, X.; Liu, P.; Xu, C.; Zhang, J.; Xu, J. Spectral Properties and Laser Operation of Nd3+-Doped Mixed Sesquioxide LuYO3 Ceramic. *J Lumin* **2021**, *238*, doi:10.1016/j.jlumin.2021.118282.
32. Li, D.; Kong, L.; Xu, X.; Liu, P.; Xie, G.; Zhang, J.; Xu, J. Spectroscopy and Mode-Locking Laser Operation of Tm:LuYO 3 Mixed Sesquioxide Ceramic. *Opt Express* **2019**, *27*, 24416–24425, doi:10.1364/oe.27.024416.
33. Pirri, A.; Maksimov, R.N.; Li, J.; Vannini, M.; Toci, G. Achievements and Future Perspectives of the Trivalent Thulium-Ion-Doped Mixed-Sesquioxide Ceramics for Laser Applications. *Materials* **2022**, *15*, 2084, doi:10.3390/ma15062084.
34. Zhou, Z.; Guan, X.; Huang, X.; Xu, B.; Xu, H.; Cai, Z.; Xu, X.; Liu, P.; Li, D.; Zhang, J.; et al. Tm^3+-Doped LuYO_3 Mixed Sesquioxide Ceramic Laser: Effective 205 Mm Source Operating in Continuous-Wave and Passive Q-Switching Regimes. *Opt Lett* **2017**, *42*, 3781, doi:10.1364/ol.42.003781.
35. Zhao, Y.; Wang, L.; Chen, W.; Pan, Z.; Wang, Y.; Liu, P.; Xu, X.; Liu, Y.; Shen, D.; Zhang, J.; et al. SESAM Mode-Locked Tm:LuYO 3 Ceramic Laser Generating 54-Fs Pulses at 2048 Nm. *Appl Opt* **2020**, *59*, 10493–10497, doi:10.1364/ao.408650.
36. Jing, W.; Loiko, P.; Serres, J.M.; Wang, Y.; Kifle, E.; Vilejshikova, E.; Aguiló, M.; Díaz, F.; Griebner, U.; Huang, H.; et al. Synthesis, Spectroscopic Characterization and Laser Operation of Ho3+ in “Mixed” (LuSc)2O3 Ceramics. *J Lumin* **2018**, *203*, doi:10.1016/j.jlumin.2018.06.043.
37. García-Cortés, A.; Zaldo, C.; Cascales, C.; Mateos, X.; Petrov, V. Laser Operation of Yb^3+ in Disordered Li_0.75Gd_0.75Ba_0.5(MoO_4)_2 Crystal with Small Quantum Defect. *Opt Express* **2007**, *15*, doi:10.1364/oe.15.018162.
38. Tokurakawa, M.; Takaichi, K.; Shirakawa, A.; Ueda, K.I.; Yagi, H.; Yanagitani, T.; Kaminskii, A.A. Diode-Pumped 188 Fs Mode-Locked Yb3+: Y2O3 Ceramic Laser. *Appl Phys Lett* **2007**, *90*, doi:10.1063/1.2476385.
39. Lupei, A.; Lupei, V.; Hau, S. Vibronics in Optical Spectra of Yb3+ and Ce3+ in YAG and Y2O3 Ceramics. *Opt Mater (Amst)* **2017**, *63*, doi:10.1016/j.optmat.2016.06.024.
40. Pirri, A.; Patrizi, B.; Maksimov, R.N.; Shitov, V.A.; Osipov, V. V.; Vannini, M.; Toci, G. Spectroscopic Investigation and Laser Behaviour of Yb-Doped Laser Ceramics Based on Mixed Crystalline Structure (ScxY1-x)2O3. *Ceram Int* **2021**, *47*, 29483–29489, doi:10.1016/j.ceramint.2021.07.116.
41. Toci, G.; Pirri, A.; Patrizi, B.; Maksimov, R.N.; Osipov, V. V.; Shitov, V.A.; Vannini, M. Yb3+:(LuxY1-x)2O3 Mixed Sesquioxide Ceramics for Laser Applications. Part II: Laser Performances. *J Alloys Compd* 2021, *853*.
42. Alimov, O.K.; Basiev, T.T.; Ashurov, M.K.; Kirpichenkova, E.O.; Murav’ev, V.B. Selective Laser Spectroscopy of Activated Crystals and Glasses. *Proceedings of GPI* **1990**, *9*.
43. Peters, V. Growth and Spectroscopy of Ytterbium-Doped Sesquioxides. *Thesis* **2001**.
44. Posener, D. The Shape of Spectral Lines: Tables of the Voigt Profile. *Australian Journal of Physics* **1959**, *12*, doi:10.1071/ph590184.
45. Gaboriaud, R.J.; Paumier, F.; Lacroix, B. Disorder-Order Phase Transformation in a Fluorite-Related Oxide Thin Film: In-Situ X-Ray Diffraction and Modelling of the Residual Stress Effects. *Thin Solid Films* **2016**, *601*, doi:10.1016/j.tsf.2015.08.030.

46. Balamurugan, S.; Rodewald, U.C.; Harmening, T.; Van Wüllen, L.; Mohr, D.; Deters, H.; Eckert, H.; Pöttgen, R. PbO / PbF2 Flux Growth of YScO3 and LaScO3 Single Crystals - Structure and Solid-State NMR Spectroscopy. *Zeitschrift fur Naturforschung - Section B Journal of Chemical Sciences* **2010**, *65*, doi:10.1515/znb-2010-1004.
47. Jeong, J.Y.; Kim, J.H. Structure and Photoluminescence of Optically Transparent Y2o3:Eu Thin Films Prepared on Sapphire Substrates by Rf Magnetron Sputtering. *Applied Science and Convergence Technology* **2021**, *30*, doi:10.5757/ASCT.2021.30.1.34.